Article

Spectral-Luminescent Properties of ZrO$_2$-Y$_2$O$_3$-Pr$_2$O$_3$ Crystals

Mikhail Borik [1], Alexey Kulebyakin [1] , Nataliya Larina [2], Elena Lomonova [1] , Dmitry Morozov [2], Valentina Myzina [1], Polina Ryabochkina [2,*] and Nataliya Tabachkova [1,3]

[1] Prokhorov General Physics Institute of the Russian Academy of Sciences, 38 Vavilov Str., 119991 Moscow, Russia

[2] Institute of Physics and Chemistry, National Research Mordovia State University, 68 Bolshevistskaya Str., 430005 Saransk, Russia

[3] Department of Materials Science of Semiconductors and Dielectrics, National University of Science and Technology (MISIS), 4 Leninskiy Prospekt, 119049 Moscow, Russia

* Correspondence: ryabochkina@freemail.mrsu.ru

Abstract: We studied the spectral-luminescent properties of $(ZrO_2)_{0.805}(Y_2O_3)_{0.188}(Pr_2O_3)_{0.007}$ and $(ZrO_2)_{0.802}(Y_2O_3)_{0.195}(Pr_2O_3)_{0.003}$ crystals grown by directional melt crystallization in a cold skull. Analysis of the absorption spectra of the crystals suggested the presence of Pr^{3+} and Pr^{4+} ions. Measurement of the relative intensities of the luminescence bands corresponding to the $^3P_0 \rightarrow {}^3H_{4,5}$, $^3P_0 \rightarrow {}^3F_{2,3,4}$, $^3P_1 \rightarrow {}^3H_5$ and $^1D_2 \rightarrow {}^3H_4$ optical transitions of the Pr^{3+} ions, and analysis of luminescence extinction kinetics for the $^3P_0$ and $^1D_2$ levels of the Pr^{3+} ions, suggests the presence of cross-relaxation $(^1D_2 \rightarrow {}^1G_4) \rightarrow (^3H_4 \rightarrow {}^3F_4)$ of the Pr^{3+} ions in the ZrO$_2$-Y$_2$O$_3$-Pr$_2$O$_3$ crystals.

Keywords: zirconia solid solutions; praseodymium ions; absorption spectrum; luminescence spectrum; cross-relaxation process

1. Introduction

Visible-wavelength solid-state lasers are intensively being developed nowadays. The interest in these lasers stems from their wide range of potential applications in various fields of science and engineering, medicine, agricultural technologies, etc. [1–6].

The trivalent praseodymium ion (Pr^{3+}) is the most widely used rare-earth ion for visible-wavelength laser generation because the structure of its energy levels provides the possibility of laser transitions in the entire visible spectral region from blue ($^3P_1 \rightarrow {}^3H_4$) to deep red ($^3P_0 \rightarrow {}^3F_3$).

Fluoride crystals are the most widely used matrix materials for solid-state visible-wavelength lasers because of the low frequency of their phonon spectrum (E = 400 cm^{-1}) which significantly reduces the rate of multiphonon non-radiative energy relaxation from the excited rare-earth ion levels in these crystals. For example, LiYF$_4$ crystals with a phonon spectrum frequency of ~460 cm^{-1} [7] are widely used. The spectral-luminescent and laser properties of Pr^{3+} ion-doped fluoride crystals have been studied before [8–20].

Oxides exhibit higher stability and mechanical strength in comparison with fluoride materials. Moreover, oxide crystals exhibit higher phonon spectrum frequencies and hence have a higher probability of non-radiative transitions. The spectral-luminescent and laser properties of some Pr^{3+} ion-doped oxide crystals have also been studied before [21–25].

Zirconia-based solid solution single crystals were obtained for the first time with the development of refractory materials technologies in the 1970s. As-crystallized cubic ZrO$_2$ undergoes a number of polymorphic transformations upon cooling. At 2340 K, there is a cubic–tetragonal transition, and at 1170 K a monoclinic modification forms. To stabilize the cubic phase of zirconia, one can introduce appropriate oxides during synthesis, such as Y$_2$O$_3$ and rare-earth (RE) oxides, as well as CaO and MgO. Many studies have dealt with the polymorphic transformations and conditions required for the stabilization of the cubic and tetragonal phases of zirconia [26–30].

Single crystals of stabilized zirconia have a number of unique physical properties. They are optically homogeneous, have a high hardness (8.5–9 Moos), and a wide spectral transmittance region (250–7500 nm). Initially, cubic single crystals of zirconia solid solutions doped with rare-earth ions were considered as active media for lamp-pumped rare-earth lasers but did not find wide application due to their low thermal conductivity. Laser diode pumping changed the requirements of the thermomechanical parameters of laser crystals, and this revived interest in zirconia single crystals. The phonon spectrum frequency of zirconia solid solutions is ~610 cm^{-1} [31–33], which is intermediate between that for $Y_3Al_5O_{12}$ crystals (~865 cm^{-1}) [7] and that for fluoride crystals (400 cm^{-1}). It should be noted that the crystalline structure of ZrO_2-based solid solutions is disordered; therefore, their absorption and luminescence spectra are broadened quite inhomogeneously. Thus, these materials can be used for the fabrication of tunable and short-pulse laser generators.

The results of semiconductor-pumped laser generation experiments for ZrO_2-Y_2O_3 crystals doped with Nd^{3+}, Tm^{3+}, Ho^{3+}, Er^{3+}, and Yb^{3+} ions have been reported previously [28–30,34–37]. However, there are no literary data on the properties of lasers based on ZrO_2-Y_2O_3 crystals doped with Pr^{3+} ions. To assess potential application domains of ZrO_2-Y_2O_3-Pr_2O_3 crystals as active media of solid-state lasers, one should carry out detailed studies of the spectral-luminescent properties of these materials. Such experiments have not yet been conducted. Therefore, the aim of this study was to assess the spectral-luminescent properties of Pr^{3+} ion-doped ZrO_2-Y_2O_3 crystals for evaluating their potential as active media for visible-wavelength lasers.

2. Materials and Methods

For the tests, ZrO_2-Y_2O_3 solid solution crystals with different Pr^{3+} ion concentrations were grown by directional melt crystallization in a cold skull with direct inductive heating on a Kristall-407 (Russia) plant at a 5 mm/h growth rate [28–30]. The as-grown crystals were transparent and had a light-green color, the intensity of which increased with the praseodymium oxide concentration. The length and cross-section of the crystals were 30–40 and 10–20 mm, respectively. Photographs of the as-grown crystals are shown in Figure 1. For elemental analysis and spectral-luminescent measurements, plane-parallel wafers were cut out from the beginning and the end sections of the crystals and polished.
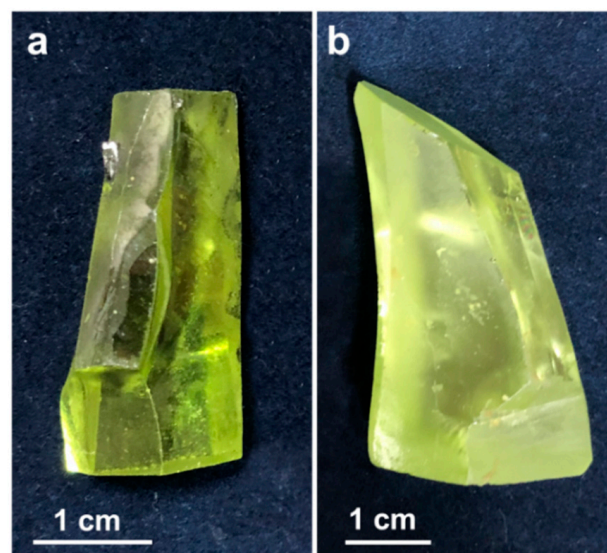
Figure 1. Photographs of as-grown crystals: (**a**) $(ZrO_2)_{0.805}(Y_2O_3)_{0.188}(Pr_2O_3)_{0.007}$; (**b**) $(ZrO_2)_{0.802}(Y_2O_3)_{0.195}(Pr_2O_3)_{0.003}$.

The $(ZrO_2)_{0.805}(Y_2O_3)_{0.188}(Pr_2O_3)_{0.007}$ and $(ZrO_2)_{0.802}(Y_2O_3)_{0.195}(Pr_2O_3)_{0.003}$ solid solution crystals had a cubic structure, as confirmed by the Raman scattering data for the crystals. By way of example, Figure 2 shows the Raman spectrum of the $ZrO_2)_{0.805}(Y_2O_3)_{0.188}(Pr_2O_3)_{0.007}$ crystal. The Raman spectrum was recorded with a Renishaw InVia (UK) spectrometer, excitation wavelength 532 nm.
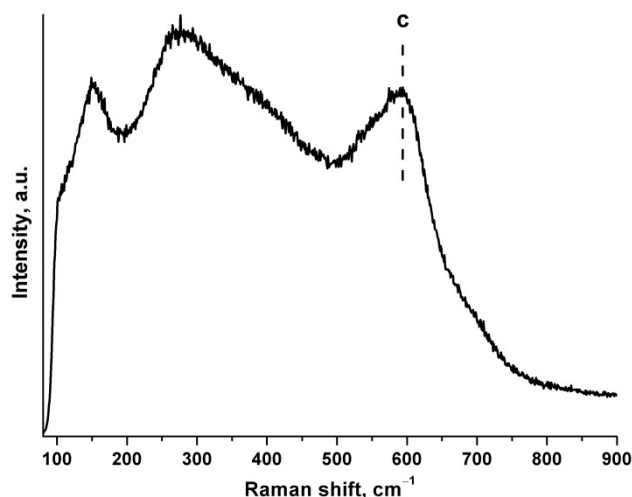
Figure 2. Raman spectrum of $(ZrO_2)_{0.805}(Y_2O_3)_{0.188}(Pr_2O_3)_{0.007}$ crystal.

The elemental composition of the crystals was determined using energy dispersion spectroscopy (EDS) with a microanalysis attachment to a Quanta TM 3D 200i electron microscope (FEI Company, Oregon, USA). Elemental analysis data are shown in Table 1.

Table 1. Elemental analysis data for test crystals.

Specimen *		ZrO_2, mol.%	Y_2O_3, mol.%	Pr_2O_3, mol.%
a	(1)	80.74 ± 0.52	18.71 ± 0.43	0.55 ± 0.10
	(2)	80.35 ± 0.54	18.87 ± 0.43	0.78 ± 0.13
b	(1)	80.65 ± 0.53	19.12 ± 0.44	0.23 ± 0.15
	(2)	79.86 ± 0.52	19.81 ± 0.45	0.33 ± 0.13

* (1) For wafer cut out from crystal beginning section; (2) for wafer cut out from crystal end section.

The Pr^{3+} ion absorption spectra of the beginning and the end of the test crystals were recorded in a double-beam scheme with a Lambda 950 spectrophotometer (Perkin Elmer, USA) at room temperature.

T = 300 K luminescence spectra were recorded with an FHR 1000 spectrophotometer (Horiba, Japan). The luminescence spectra were excited from the $^3P_2$ level to the underlying levels of the Pr^{3+} ions by a diode solid-state laser, MGL-N-457nm-1W ($\lambda_{exc.}$ = 457 nm) (CNI Laser, China). The radiation receiver was a Hamamatsu R928B photoelectron multiplier (Hamamatsu Photonics, Japan).

Extinction kinetic curves of luminescence from the $^3P_0$ and $^1D_2$ levels of the Pr^{3+} ions in the ZrO_2-Y_2O_3-Pr_2O_3 crystals were recorded with a Rohde & Schwarz RTM3004 high-resolution digital oscilloscope (Rohde & Schwarz, Germany). The recording wavelengths were 504 and 612 nm, with luminescence excitation by a Al_2O_3:Ti crystal LX 329 laser (SOLAR Laser Systems, Belarus Republic) with a 450 nm wavelength, a 15 ns pulse duration, and a 10 Hz pulse rate.

3. Results and Discussion

Elemental analysis data (Table 1) suggest an increase in the praseodymium oxide content along the crystal. The difference in the Pr_2O_3 concentrations at the beginning and the end of the crystal is caused by the fact that the Pr^{3+} ions have a relatively large radius

in comparison with that of the Zr^{4+} ions and are therefore displaced toward the end of the growing crystals.

Figure 3 shows the absorption spectra of the test ZrO_2-Y_2O_3-Pr_2O_3 crystals for (a) 350–700 and (b) 900–2500 nm ranges. The digits mark the absorption spectra of the ZrO_2-Y_2O_3-Pr_2O_3 specimens cut out from the crystal sections corresponding to (1) the beginning of growth and (2) end of growth.
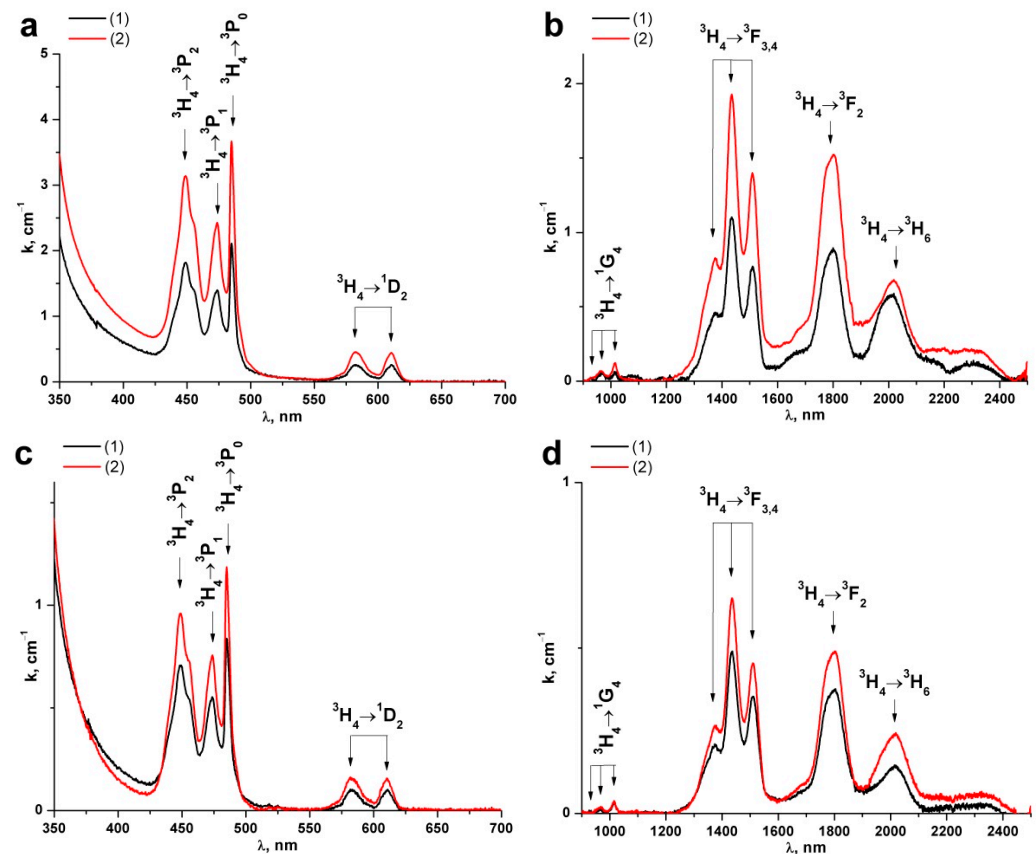
Figure 3. Absorption spectra of Pr^{3+}/Pr^{4+} ions in the crystals: (**a,b**) $(ZrO_2)_{0.805}(Y_2O_3)_{0.188}(Pr_2O_3)_{0.007}$; (**c,d**) $(ZrO_2)_{0.802}(Y_2O_3)_{0.195}(Pr_2O_3)_{0.003}$; (1) beginning of growth and (2) end of growth.

The absorption spectra of the ZrO_2-Y_2O_3-Pr_2O_3 crystals contain bands corresponding to the $4f$–$4f$ intra-configurational optical transitions of the Pr^{3+} ions from the main state $^3H_4$ to the $^3P_2$, $^3P_1$, $^3P_0$, $^1D_2$, $^1G_4$, $^3F_{2,3,4}$, and $^3H_6$ excited multiplets. These bands are broadened quite inhomogeneously due to the disordering of the crystal structure.

It is noteworthy that the absorption bands of the Pr^{3+} ions are resolved against the tail of a wide band, which seems to originate from the presence of Pr^{4+} ions in the ZrO_2-Y_2O_3-Pr_2O_3 crystals. The presence of both trivalent and tetravalent praseodymium ions in the ZrO_2-Y_2O_3-Pr_2O_3 crystals has been reported before [28,29,38,39].

Analysis of the absorption spectra shown in Figure 3 revealed that the intensity of the Pr^{3+} ion-related absorption bands increases as one moves toward the end of the crystal.

Comparing the absorption spectra of the Pr^{3+}/Pr^{4+} ions in the ZrO_2-Y_2O_3-Pr_2O_3 crystals containing different concentrations of praseodymium ions was also of interest. Figure 4 shows the absorption spectra of the Pr^{3+}/Pr^{4+} ions in the $(ZrO_2)_{0.805}(Y_2O_3)_{0.188}(Pr_2O_3)_{0.007}$ and $(ZrO_2)_{0.802}(Y_2O_3)_{0.195}(Pr_2O_3)_{0.003}$ crystals recorded under similar conditions.
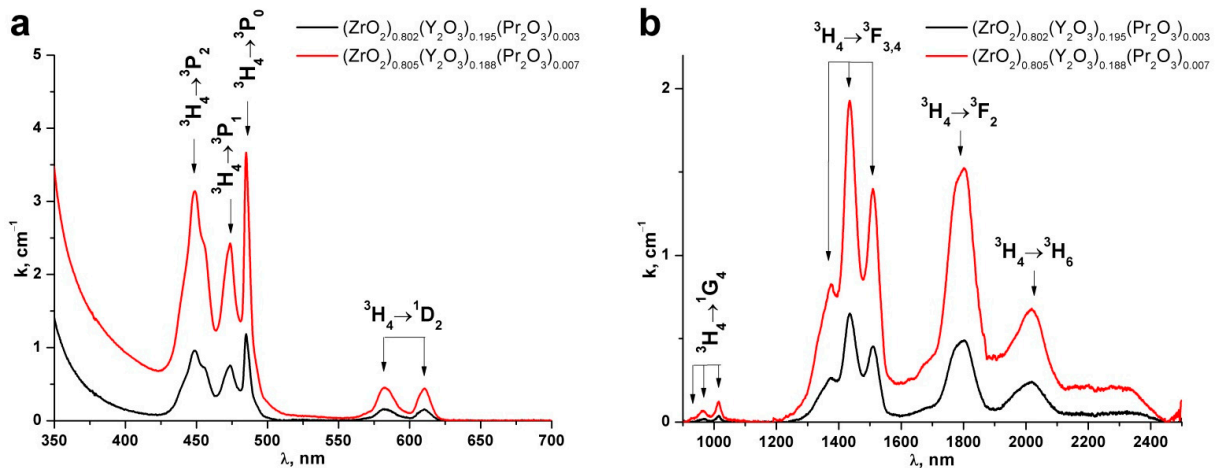
Figure 4. Absorption spectra of Pr^{3+}/Pr^{4+} ions in $(ZrO_2)_{0.805}(Y_2O_3)_{0.188}(Pr_2O_3)_{0.007}$ and $(ZrO_2)_{0.802}(Y_2O_3)_{0.195}(Pr_2O_3)_{0.003}$ crystals recorded in (**a**) 350–700 and (**b**) 900–2500 nm ranges.

Analysis of the absorption spectra shown in Figure 4 suggests that both the Pr^{3+} and Pr^{4+} ion absorption band intensities for the $(ZrO_2)_{0.805}(Y_2O_3)_{0.188}(Pr_2O_3)_{0.007}$ crystal are higher than those of the respective bands for the $(ZrO_2)_{0.802}(Y_2O_3)_{0.195}(Pr_2O_3)_{0.003}$ crystal.

The luminescence spectra for the $^3P_0 \rightarrow {}^3H_{4,5}$, $^3P_0 \rightarrow {}^3F_{2,3,4}$, $^3P_1 \rightarrow {}^3H_5$, and $^1D_2 \rightarrow {}^3H_4$ optical transitions of the Pr^{3+} ions for different crystal ZrO_2-Y_2O_3-Pr_2O_3 sections, recorded with laser excitation at $\lambda_{exc.} = 457$ nm at T = 300 K, are shown in Figure 5. The digits mark the luminescence spectra of the ZrO_2-Y_2O_3-Pr_2O_3 specimens cut out from the crystal sections corresponding to (1) beginning of growth and (2) end of growth.
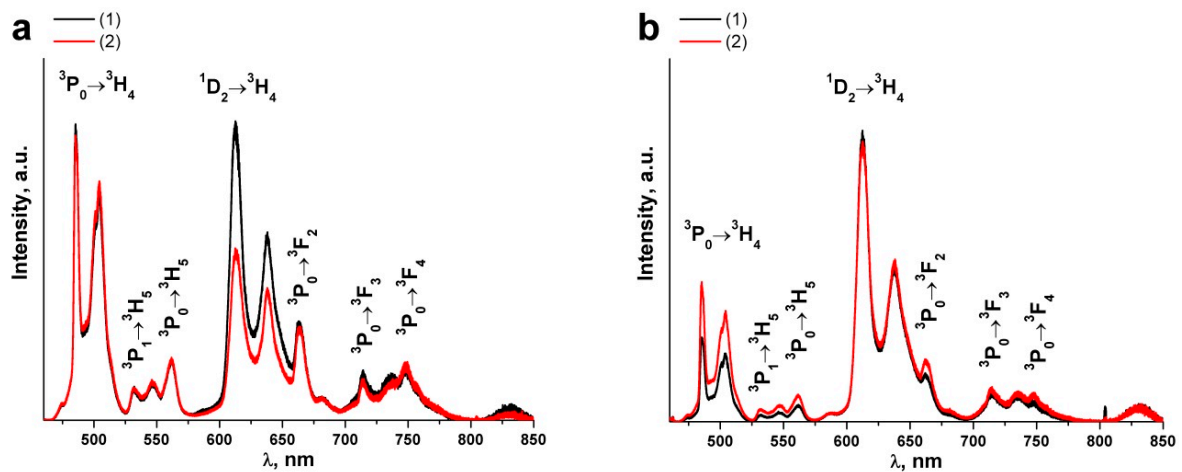
Figure 5. Luminescence spectra of Pr^{3+} ions in the crystals: (**a**) $(ZrO_2)_{0.805}(Y_2O_3)_{0.188}(Pr_2O_3)_{0.007}$; (**b**) $(ZrO_2)_{0.802}(Y_2O_3)_{0.195}(Pr_2O_3)_{0.003}$; (1) beginning of crystal and (2) end of crystal, $\lambda_{exc.} = 457$ nm, T = 300 K.

The significant inhomogeneous broadening in the luminescence spectra of Pr^{3+} ions in ZrO_2-Y_2O_3-Pr_2O_3 is caused by the disordering of the crystal structure.

It can be seen from Figure 5 that the luminescence spectra of the Pr^{3+} ions taken from different crystal sections exhibit a redistribution of the relative intensities of the $^3P_0 \rightarrow {}^3H_4$ and $^1D_2 \rightarrow {}^3H_4$ optical transition bands. In the luminescence spectrum taken at the beginning of the $(ZrO_2)_{0.805}(Y_2O_3)_{0.188}(Pr_2O_3)_{0.007}$ crystal, the relative intensity of the $^3P_0 \rightarrow {}^3H_4$ transition bands is comparable with that of the $^1D_2 \rightarrow {}^3H_4$ transition bands. However, in the luminescence spectrum taken at the end of the crystal, the intensity of the $^1D_2 \rightarrow {}^3H_4$ transition bands decreases relative to that of the $^3P_0 \rightarrow {}^3H_4$ transition bands. For the $(ZrO_2)_{0.802}(Y_2O_3)_{0.195}(Pr_2O_3)_{0.003}$ crystal with a lower praseodymium concentration,

the relative intensity of the $^3P_0 \to {}^3H_4$ transition bands is lower than that of the $^1D_2 \to {}^3H_4$ transition bands. There is also a trend of decreasing intensity of the $^1D_2 \to {}^3H_4$ transition bands relative to that of the $^3P_0 \to {}^3H_4$ transition bands in the luminescence spectrum taken from the crystal section corresponding to the end of growth. The trend of decreasing intensity of the $^1D_2 \to {}^3H_4$ transition bands in comparison with that of the $^3P_0 \to {}^3H_4$ transition bands is also observed in the luminescence spectra of the crystals with a higher concentration of Pr^{3+} ions (Figure 6).
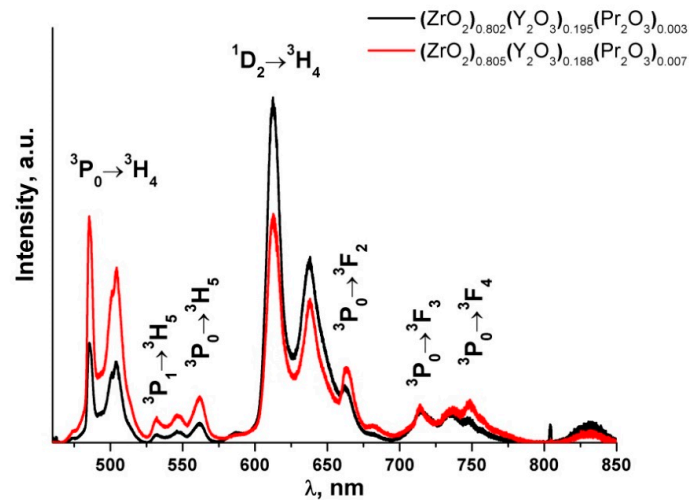
Figure 6. Luminescence spectra of Pr^{3+} ions in $(ZrO_2)_{0.802}(Y_2O_3)_{0.195}(Pr_2O_3)_{0.003}$ and $(ZrO_2)_{0.805}(Y_2O_3)_{0.188}(Pr_2O_3)_{0.007}$ crystals.

This redistribution of the relative luminescence band intensities for the $^3P_0 \to {}^3H_4$ and $^1D_2 \to {}^3H_4$ optical transitions of the Pr^{3+} ions has been observed before for $La_{1-x}Pr_xGa_{0.5}Sb_{1.5}O_6$ and YPO_4 particles and $BaGd_2(MoO_4)_4$ crystals doped with Pr^{3+} ions [40–42].

The redistribution of the relative luminescence band intensities for the $^3P_0 \to {}^3H_4$ and $^1D_2 \to {}^3H_4$ optical transitions of the Pr^{3+} ions was attributed by the authors [40–42] to the presence of cross-relaxation of the Pr^{3+} ions $(^1D_2 \to {}^1G_4) \to (^3H_4 \to {}^3F_4)$, as shown in Figure 7.
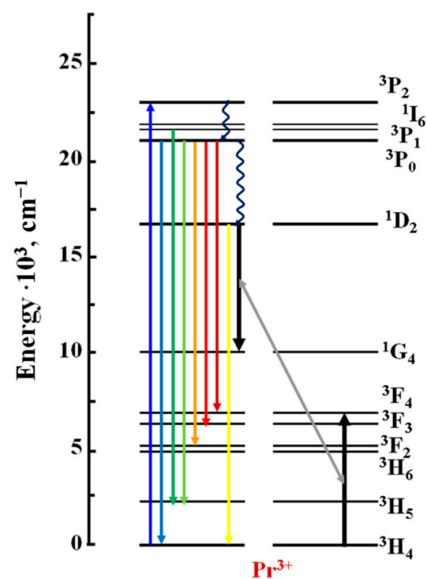
Figure 7. Schematic of energy levels of Pr^{3+} ions showing the cross-relaxation process $(^1D_2 \to {}^1G_4) \to (^3H_4 \to {}^3F_4)$ for these ions (black arrows). The arrow color determines the corresponding spectral range of optical transitions.

The redistribution of the relative luminescence band intensities for the $^3P_0 \rightarrow {}^3H_4$ and $^1D_2 \rightarrow {}^3H_4$ optical transitions of the Pr^{3+} ions in the luminescence spectra of the $(ZrO_2)_{0.802}(Y_2O_3)_{0.195}(Pr_2O_3)_{0.003}$ and $(ZrO_2)_{0.805}(Y_2O_3)_{0.188}(Pr_2O_3)_{0.007}$ crystals revealed in this study is also attributable to the presence of non-radiative energy exchange between the Pr^{3+} ions in the excited state $^1D_2$ and the Pr^{3+} ions in the main state $^3H_4$.

In order to confirm this assumption, extinction kinetic curves of luminescence from the $^3P_0$ and $^1D_2$ levels of the Pr^{3+} ions in the $(ZrO_2)_{0.802}(Y_2O_3)_{0.195}(Pr_2O_3)_{0.003}$ and $(ZrO_2)_{0.805}(Y_2O_3)_{0.188}(Pr_2O_3)_{0.007}$ crystals were recorded. Figure 8 shows the 504 and 612 nm luminescence extinction kinetic curves for these levels (excitation by second harmonic of an Al_2O_3:Ti crystal laser, 450 nm wavelength, 15 ns pulse duration, 10 Hz pulse rate).
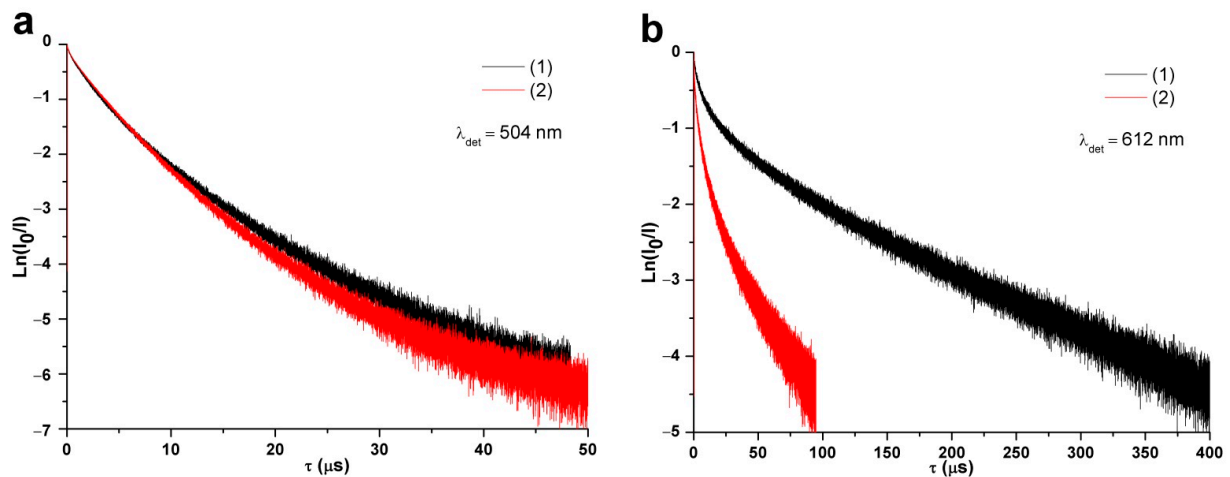
Figure 8. Extinction kinetic curves of luminescence from the $^3P_0$ and $^1D_2$ levels of the Pr^{3+} ions in (1) $(ZrO_2)_{0.802}(Y_2O_3)_{0.195}(Pr_2O_3)_{0.003}$ and (2) $(ZrO_2)_{0.805}(Y_2O_3)_{0.188}(Pr_2O_3)_{0.007}$ crystals, $\lambda_{exc.}$ = 450 nm, (**a**) $\lambda_{det.}$ = 504 nm, (**b**) $\lambda_{det.}$ = 612 nm.

It can be seen from Figure 8a that the $^3P_0$ level luminescence extinction curves are non-exponential both for the $(ZrO_2)_{0.802}(Y_2O_3)_{0.195}(Pr_2O_3)_{0.003}$ and the $(ZrO_2)_{0.805}(Y_2O_3)_{0.188}(Pr_2O_3)_{0.007}$ crystals. With an increase in the Pr^{3+} ion concentration in the test crystals, the curve patterns change, but only slightly. Therefore, the non-exponential pattern of the respective decomposition curves can be attributed either to the presence of various optical centers of the Pr^{3+} ions differing in the $^3P_0$ level lifetime or to the interaction between the Pr^{3+} and the Pr^{4+} ions.

The $^1D_2$ level luminescence extinction kinetic curves for the $(ZrO_2)_{0.802}(Y_2O_3)_{0.195}(Pr_2O_3)_{0.003}$ and $(ZrO_2)_{0.805}(Y_2O_3)_{0.188}(Pr_2O_3)_{0.007}$ crystals (Figure 8b) are also non-exponential. However, with an increase in the Pr^{3+} ion concentration in these crystals, the decomposition of the $^1D_2$ level becomes faster, confirming the earlier assumption of the presence of non-radiative energy transfer between the Pr^{3+} ions $(^1D_2 \rightarrow {}^1G_4) \rightarrow (^3H_4 \rightarrow {}^3F_4)$. The non-exponential pattern of the $^1D_2$ level luminescence kinetics for the $(ZrO_2)_{0.802}(Y_2O_3)_{0.195}(Pr_2O_3)_{0.003}$ crystals seems to originate from the non-radiative energy transfer as per the schematic Pr^{3+} $(^1D_2 \rightarrow {}^1S_0) \rightarrow (^1D_2 \rightarrow {}^3H_4)$.

The presence of non-radiative energy transfer between the Pr^{3+} ions $(^1D_2 \rightarrow {}^1G_4) \rightarrow (^3H_4 \rightarrow {}^3F_4)$ is confirmed by the pattern of the $^3P_0$ and $^1D_2$ level luminescence extinction curves for the Pr^{3+} ions taken from the beginning and the end of the $(ZrO_2)_{0.805}(Y_2O_3)_{0.188}(Pr_2O_3)_{0.007}$ crystals (Figure 9).
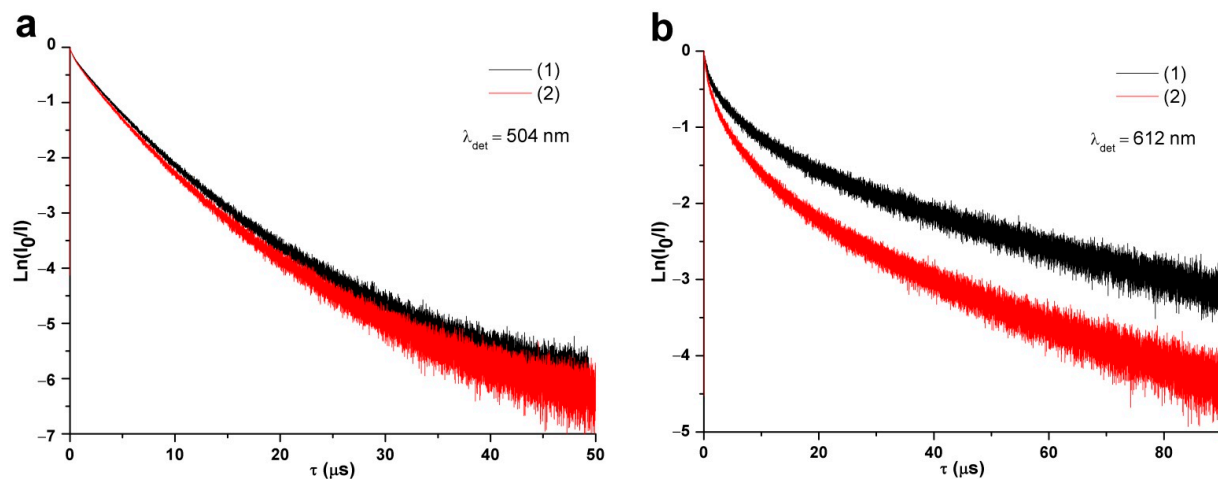
Figure 9. Extinction kinetic curves of luminescence from $^3P_0$ and $^1D_2$ levels of Pr^{3+} ions for $(ZrO_2)_{0.805}(Y_2O_3)_{0.188}(Pr_2O_3)_{0.007}$ crystal, $\lambda_{exc.} = 450$ nm, T = 300 K: (**a**) $\lambda_{det.} = 504$ nm, (**b**) $\lambda_{det.} = 612$ nm; (1) beginning of crystal and (2) end of crystal.

4. Summary

In this study, $(ZrO_2)_{0.802}(Y_2O_3)_{0.195}(Pr_2O_3)_{0.003}$ and $(ZrO_2)_{0.805}(Y_2O_3)_{0.188}(Pr_2O_3)_{0.007}$ solid solution single crystals were synthesized by directional melt crystallization in a cold skull. The spectral-luminescent properties of praseodymium ions in these crystals were studied in detail for the first time. Analysis of the absorption spectra of the $(ZrO_2)_{0.803}(Y_2O_3)_{0.190}(Pr_2O_3)_{0.007}$ and $(ZrO_2)_{0.804}(Y_2O_3)_{0.193}(Pr_2O_3)_{0.003}$ crystals suggests the presence of both Pr^{3+} and Pr^{4+} ions in the crystals. Analysis of the luminescence spectra and the $^3P_0$ and $^1D_2$ level luminescence extinction curves for Pr^{3+} ions in the test crystals revealed the presence of concentration quenching of the luminescence from the excited state $^1D_2$ in the Pr^{3+} ions due to cross-relaxation $(^1D_2 \rightarrow \, ^1G_4) \rightarrow (^3H_4 \rightarrow \, ^3F_4)$.

Author Contributions: Conceptualization, P.R.; methodology, P.R.; investigation, N.L., D.M.; resources, M.B., E.L., A.K., V.M., and N.T.; writing—review and editing, N.L., P.R., and D.M.; visualization, N.L., D.M. All authors have read and agreed to the published version of the manuscript.

Conflicts of Interest: The authors declare no conflict of interest.

References

1. Zou, J.; Ruan, Q.; Zhang, X.; Xu, B.; Cai, Z.; Luo, Z. Visible-wavelength pulsed lasers with low-dimensional saturable absorbers. *Nanophotonics* **2020**, *9*, 2273–2294. [CrossRef]
2. Lin, J.-T. Progress of medical lasers: Fundamentals and applications. *Med. Devices Diagn. Eng.* **2016**, *2*, 36–41. [CrossRef]
3. Nadimi, M.; Sun, D.W.; Paliwal, J. Recent applications of novel laser techniques for enhancing agricultural production. *Laser Phys.* **2021**, *31*, 053001. [CrossRef]
4. Huber, G. Advances in Solid-State Laser Materials. *ECS Trans.* **2009**, *25*, 287–290. [CrossRef]
5. Finlayson, D.M.; Sinclair, B.D.; Osborne, P. *Advances in Lasers and Applications: Proceedings of the Fifty Second Scottish Universities Summer School in Physics*; CRC Press: Boca Raton, FL, USA, 1998; 346p. [CrossRef]
6. Kränkel, C.; Marzahl, D.-T.; Moglia, F.; Huber, G.; Metz, P.W. Out of the blue: Semiconductor laser pumped visible rare-earth doped lasers. *Laser Photonics Rev.* **2016**, *10*, 548–568. [CrossRef]
7. Moncorge, R. Laser crystals with low phonon frequencies. *Ann. Chim.-Sci. Mat.* **2003**, *28*, 5–20. [CrossRef]
8. Richter, A.; Heumann, E.; Osiac, E.; Huber, G.; Seelert, W.; Diening, A. Diode pumping of a continuous-wave Pr^{3+}-doped $LiYF_4$ laser. *Opt. Lett.* **2004**, *29*, 2638–2640. [CrossRef]
9. Liu, Z.; Cai, Z.; Huang, S.; Zeng, C.; Meng, Z.; Bu, Y.; Luo, Z.; Xu, B.; Xu, H.; Ye, C.; et al. Diode-pumped Pr^{3+}:$LiYF_4$ continuous-wave deep red laser at 698 nm. *J. Opt. Soc. Am. B* **2013**, *30*, 302–305. [CrossRef]

10. Luo, S.; Xu, B.; Cui, S.; Chen, H.; Cai, Z.; Xu, H. Diode-pumped continuous-wave dual-wavelength c-cut Pr^{3+}:LiYF$_4$ laser at 696 and 719 nm. *Appl. Opt.* **2015**, *54*, 10051–10054. [CrossRef]

11. Li, X.D.; Yu, X.; Yan, R.P.; Fan, R.W.; Chen, D.Y. Optical and laser properties of Pr^{3+}:YLF crystal. *Laser Phys. Lett.* **2011**, *8*, 791–794. [CrossRef]

12. Cao, W.; Li, Z.; Shi, C.; Lin, J.; Lin, X.; Xu, G.; Xu, H.; Cai, Z. Overview of research and development of Pr^{3+} doped solid-state lasers. *Opto-Electron. Eng.* **2022**, *49*, 210364. [CrossRef]

13. Richter, A.; Heumann, E.; Huber, G.; Ostroumov, V.; Seelert, W. Power scaling of semiconductor laser pumped Praseodymium-lasers. *Opt. Express* **2007**, *15*, 5172–5178. [CrossRef] [PubMed]

14. Xu, B.; Camy, P.; Doualan, J.-L.; Cai, Z.; Moncorgé, R. Visible laser operation of Pr^{3+}-doped fluoride crystals pumped by a 469 nm blue laser. *Opt. Express* **2011**, *19*, 1191–1197. [CrossRef] [PubMed]

15. Cornacchia, F.; Di Lieto, A.; Tonelli, M.; Richter, A.; Heumann, E.; Huber, G. Efficient visible laser emission of GaN laser diode pumped Pr-doped fluoride scheelite crystals. *Opt. Express* **2008**, *16*, 15932–15941. [CrossRef]

16. Metz, P.W.; Müller, S.; Reichert, F.; Marzahl, D.T.; Moglia, F.; Kränkel, C.; Huber, G. Wide wavelength tunability and green laser operation of diode-pumped Pr^{3+}:KY$_3$F$_{10}$. *Opt. Express* **2013**, *16*, 31274–31281. [CrossRef] [PubMed]

17. Reichert, F.; Moglia, F.; Marzahl, D.-T.; Metz, P.; Fechner, M.; Hansen, N.-O.; Huber, G. Diode pumped laser operation and spectroscopy of Pr^{3+}:LaF$_3$. *Opt. Express* **2012**, *20*, 20387–20395. [CrossRef]

18. Paboeuf, D.; Mhibik, O.; Bretenaker, F.; Goldner, P.; Parisi, D.; Tonelli, M. Diode-pumped Pr:BaY$_2$F$_8$ continuous-wave orange laser. *Opt. Lett.* **2011**, *36*, 280–282. [CrossRef]

19. Sottile, A.; Metz, P.W. Deep red diode-pumped Pr^{3+}:KY$_3$F$_{10}$ continuous-wave laser. *Opt. Lett.* **2015**, *40*, 1992–1995. [CrossRef]

20. Yu, H.; Jiang, D.; Tang, F.; Su, L.; Luo, S.; Yan, X.; Xu, B.; Cai, Z.; Wang, J.; Ju, Q.; et al. Enhanced photoluminescence and initial red laser operation in Pr:CaF$_2$ crystal via co-doping Gd^{3+} ions. *Mater. Lett.* **2017**, *206*, 140–142. [CrossRef]

21. Fibrich, M.; Jelínková, H.; Šulc, J.; Nejezchleb, K.; Škoda, V. Visible cw laser emission of GaN-diode pumped Pr:YAlO$_3$ crystal. *Appl. Phys. B* **2009**, *97*, 363–367. [CrossRef]

22. Fechner, M.; Reichert, F.; Hansen, N.-O.; Petermann, K.; Huber, G. Crystal growth, spectroscopy, and diode pumped laser performance of Pr, Mg:SrAl$_{12}$O$_{19}$. *Appl. Phys. B* **2011**, *102*, 731–735. [CrossRef]

23. Zhou, S.; Pan, Y.; Li, N.; Xu, B.; Liu, J.; Song, Q.; Xu, J.; Li, D.; Liu, P.; Xu, X.; et al. Spectroscopy and diode-pumped laser operation of Pr:LaMgAl$_{11}$O$_{19}$ crystal. *Opt. Mater.* **2019**, *89*, 14–17. [CrossRef]

24. Fujita, S.; Tanaka, H.; Kannari, F. Output characteristics of Pr:YAlO$_3$ and Pr:YAG lasers pumped by high-power GaN laser diodes. *Appl. Opt.* **2020**, *59*, 5124–5130. [CrossRef] [PubMed]

25. Li, Q.; Wang, Y.; Wang, J.; Ma, J.; Ni, M.; Lin, H.; Zhang, J.; Liu, P.; Xu, X.; Tang, D. High transparency Pr:Y$_2$O$_3$ ceramics: A promising gain medium for red emission solid-state lasers. *J. Adv. Ceram.* **2022**, *11*, 874–881. [CrossRef]

26. Rouanet, A. High temperature solidification and phase diagrams of the ZrO$_2$-Er$_2$O$_3$, ZrO$_2$-Y$_2$O$_3$ and ZrO$_2$-Yb$_2$O$_3$ systems. *CR Seances Acad. Sci.* **1968**, *267*, 1581.

27. Srivastava, K.K.; Patil, R.N.; Choudhary, C.B.; Gokhale, K.V.G.K.; Subbarao, E.C. Revised phase diagram of the system ZrO$_2$-YO$_{1.5}$. *Trans. J. Br. Ceram. Soc.* **1974**, *73*, 85–91.

28. Kuz'minov, Y.S.; Lomonova, E.E.; Osiko, V.V. *Cubic Zirconia and Skull Melting*; Cambridge International Science Publishing Ltd.: Cambridge, UK, 2009; 346p.

29. Osiko, V.W.; Borik, M.A.; Lomonova, E.E. Synthesis of Refractory Materials by Skull Melting Technique. In *Springer Handbook of Crystal Growth*; Springer Science and Business Media LLC: Berlin/Heidelberg, Germany, 2010; pp. 433–477.

30. Aleksandrov, V.I.; Osiko, V.V.; Prokhorov, A.M.; Tatarintsev, V.M. The Formation of High-temperature Materials by Direct High-frequency Fusion in a Cold Container. *Russ. Chem. Rev.* **1978**, *47*, 385–427. [CrossRef]

31. Jana, S.; Biswas, P.K. Characterization of oxygen deficiency and trivalent zirconium in sol-gel derived zirconia films. *Mater. Lett.* **1997**, *30*, 53–58. [CrossRef]

32. Foltin, M.; Stueber, G.J.; Bernstein, E.R. Investigation of the structure, stability, and ionization dynamics of zirconium oxide clusters. *J. Phys. Chem.* **2005**, *114*, 8971–8989. [CrossRef]

33. Pomfret, M.B.; Stoltz, C.; Varughese, B.; Walker, R.A. Structural and Compositional Characterization of Yttria-Stabilized Zirconia: Evidence of Surface- Stabilized, Low-Valence Metal Species. *Anal. Chem.* **2005**, *77*, 1791–1795. [CrossRef]

34. Borik, M.A.; Lomonova, E.E.; Malov, A.V.; Kulebyakin, A.V.; Ryabochkina, P.A.; Ushakov, S.N.; Uslamina, M.A.; Chabushkin, A.N. Spectral, luminescent, and lasing properties of ZrO$_2$-Y$_2$O$_3$-Tm$_2$O$_3$ crystals. *Quantum Electron.* **2012**, *42*, 580–582. [CrossRef]

35. Borik, M.A.; Lomonova, E.E.; Lyapin, A.A.; Kulebyakin, A.V.; Ryabochkina, P.A.; Ushakov, S.N.; Chabushkin, A.N. Lasing characteristics of ZrO$_2$-Y$_2$O$_3$-Ho$_2$O$_3$ crystal. *Quantum Electron.* **2013**, *43*, 838–840. [CrossRef]

36. Ryabochkina, P.A.; Sidorova, N.V.; Chabushkin, A.N.; Lomonova, E.E. Lasing at the $^4I_{13/2} \rightarrow {}^4I_{15/2}$ transition of Er^{3+} ions in ZrO$_2$-Y$_2$O$_3$-Er$_2$O$_3$ crystals under resonant diode pumping into the $^4I_{13/2}$ level. *Quantum Electron.* **2016**, *46*, 451–452. [CrossRef]

37. Voronko, Y.K.; Lomonova, E.E.; Osiko, V.V.; Sobol, A.A.; Ushakov, S.N.; Shukshin, V.E. Active laser media based on fianite crystals. *Quantum Electron.* **2006**, *36*, 601–608. [CrossRef]

38. Kunz, M.; Kretschmann, H.; Assmus, W.; Klingshirn, C. Absorption and emission spectra of yttria-stabilized zirconia and magnesium oxide. *J. Lumin.* **1987**, *37*, 123–131. [CrossRef]

39. Savoini, B.; Munoz Santiuste, J.E.; Gonzalez, R. Optical characterization of Pr^{3+}-doped yttria-stabilized zirconia single crystals. *Phys. Rev. B* **1997**, *56*, 5856–5865. [CrossRef]

40. Egorysheva, A.V.; Gajtko, O.M.; Golodukhina, S.V.; Khrushchalina, S.A.; Ryabochkina, P.A.; Taratynova, A.D.; Yurlov, I.A. Synthesis and spectral-luminescent properties of $La_{1-x}Pr_xGa_{0.5}Sb_{1.5}O_6$ solid solutions. *Ceram. Int.* **2019**, *45*, 16886–16892. [CrossRef]

41. Chen, H.; Lian, R.; Yin, M.; Lou, L.; Zhang, W.; Xia, S.; Krupa, J.-C. Luminescence concentration quenching of $^1D_2$ state in $YPO_4:Pr^{3+}$. *J. Phys. Condens. Matter.* **2001**, *13*, 1151–1158. [CrossRef]

42. Guan, Y.; Tsuboi, T.; Huang, Y.; Huang, W. Concentration quenching of praseodymium ions Pr^{3+} in $BaGd_2(MoO_4)_4$ crystals. *Dalton Trans.* **2014**, *43*, 3698–3703. [CrossRef]